1882 *Biochemistry* **2010,** *49,* 1882–1892
DOI: 10.1021/bi901922t

BIOCHEMISTRY
including biophysical chemistry & molecular biology
Article

Structural and Spectroscopic Consequences of Hexacoordination of a Bacteriochlorophyll Cofactor in the *Rhodobacter sphaeroides* Reaction Center[†,‡]

Dmitrij Frolov,[§] May Marsh,[∥,@] Lucy I. Crouch,[∥] Paul K. Fyfe,[∥,#] Bruno Robert,[⊥] Rienk van Grondelle,[§] Andrea Hadfield,[∥] and Michael R. Jones*[,∥]

[§]*Department of Physics and Astronomy, Free University of Amsterdam, De Boelelaan 1081, 1081 HV Amsterdam, The Netherlands,* [∥]*Department of Biochemistry, School of Medical Sciences, University of Bristol, University Walk, Bristol BS8 1TD, United Kingdom, and* [⊥]*Service de Biophysique des Fonctions Membranaires, DBJC/CEA and URA 2096/CNRS, CEA-Saclay, F-91191 Gif-sur-Yvette, France* [@]*Present address: Department of Biochemistry, University of Cambridge, 80 Tennis Court Rd., Cambridge CB2 1GA, United Kingdom.* [#]*Present address: Division of Biological Chemistry and Drug Discovery, Faculty of Life Sciences, University of Dundee, Nethergate, Dundee DD1 4HN, United Kingdom.*

Received November 9, 2009; Revised Manuscript Received January 28, 2010

ABSTRACT: The structural and functional consequences of changing the coordination state of one of the bacteriochlorophyll (BChl) cofactors in the purple bacterial reaction center have been explored. A combination of steady state spectroscopy and X-ray crystallography was used to demonstrate that mutagenesis of residue 181 of the L-polypeptide from Phe to Arg (FL181R) causes the BChl at the accessory (B_B) position on the so-called inactive cofactor branch to become hexacoordinated, with no significant changes to the structure of the surrounding protein. This change was accompanied by the appearance of a distinctive absorbance band at 631 nm in the room-temperature absorbance spectrum. The ligand donor was not the Arg side chain but rather an intervening water molecule, and contrary to expectations, the Mg of B_B did not adopt a more in-plane geometry in response to hexacoordination. The mutation caused a disturbance to the detailed conformation of the BChl macrocycle that manifested in a number of subtle changes to the resonance Raman spectrum. Hexacoordination of B_B produced a small increase in the lifetime of the excited electronic state of the primary donor bacteriochlorophylls (P*), indicating some disturbance to light-driven energy and/or electron transfer events on the time scale of a few picoseconds after light excitation. The B_B bacteriochlorophyll returned to a pentacoordinated state in a double mutant where the FL181R mutation was combined with removal of the native axial ligand through mutation of His M182 to Leu. Experimental evidence of hexacoordinated bacteriochlorophylls in the literature on antenna proteins is considered, and possible reasons why hexacoordinated bacteriochlorophylls and chlorophylls appear to be avoided in photosynthetic proteins are discussed.

Photosynthetic systems based on chlorophyll (Chl)[1] use light energy to power a series of electron transfer reactions that are linked to proton translocation across a charge impermeable membrane. The Chl cofactors have two principal roles, acting as light-harvesting pigments in the antenna and as electron carriers in the reaction centers (RCs) of the electron transfer chain. Chl is a magnesium tetrapyrrole, the central Mg atom being coordinated to the four nitrogen atoms of the macrocycle. A variety of Chl types are known, varying in the substituent groups attached to the four pyrrole rings (*1*), and anoxygenic photosynthetic bacteria possess a number of related bacteriochlorophyll (BChl) pigments (*1*, *2*). The structure of the macrocycle of BChl *a* is shown in Figure 1A. In pheophytin *a* and bacteriopheophytin *a* (BPhe *a*), specialist pigments found in type II RCs, the Mg is replaced with two hydrogen ions (*1*).

In organic solvent, the Mg of BChl or Chl [denoted (B)Chl] can be either penta- or hexacoordinated, depending on the polarity of the solvent, with the fifth and sixth ligands arranged perpendicular to, and on either side of, the plane of the (B)Chl macrocycle (termed axial ligands). In proteins, a pentacoordinated state appears to be very strongly favored, with a single axial ligand donated to one side of the macrocycle by a suitable donor group. An example, taken from the *Rhodobacter sphaeroides* RC, is shown in Figure 1A. The most commonly observed ligand donor in structurally characterized (B)Chl-containing proteins is a His residue or water molecule, but the side chains of Asn, Gln, Asp, Glu, Met, and Tyr can also act as ligand donors, along with the oxygen of a backbone carbonyl or a lipid phosphodiester group (*3*−*11*). As defined elsewhere (*12*), the ligand can be either in an *anti* configuration with the ligand donor on the opposite side of the BChl macrocycle from the phytol chain (as shown in Figure 1A) or in a *syn* configuration with the ligand donor on the

[†]This work was supported by The Netherlands Organization for Scientific Research (NWO) via the Dutch Foundation for Earth and Life Sciences (ALW) (D.F. and R.v.G.) and by the Biotechnology and Biological Sciences Research Council of the United Kingdom and the University of Bristol (M.R.J., P.K.F., L.I.C., M.M., and A.H.).

[‡]The X-ray crystal structure of the FL181R RC has been deposited in the Protein Data Bank as entries 2wx5 (coordinates) and r2wx5sf (structure factors).

*To whom correspondence should be addressed. Phone: 00-44-117-3312135. Fax: 00-44-117-3312168. E-mail: m.r.jones@bristol.ac.uk.

[1]Abbreviations: BChl, bacteriochlorophyll; BPhe, bacteriopheophytin; Chl, chlorophyll; Et_2O, diethyl ether; FMO, Fenna−Matthews−Olson; LDAO, lauryl dimethylamine oxide; SADS, species-associated difference spectra; THF, tetrahydrofuran; P, primary donor of electrons; rmsd, root-mean-square deviation.

 Published on Web 01/29/2010

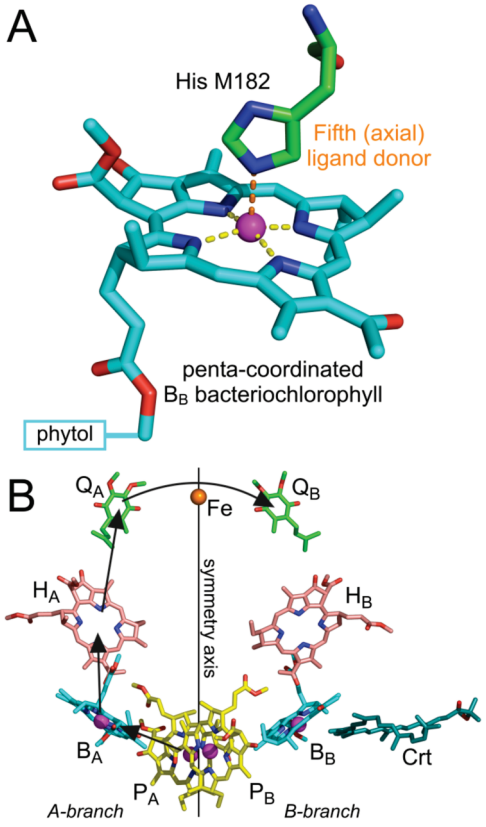

FIGURE 1: Structure of pentacoordinated BChl *a* and cofactor organization in the *Rba. sphaeroides* RC. (A) Stick model of the macrocycle of the B_B BChl (cyan carbons, blue nitrogens, and red oxygens), in which the phytol side chain (bottom left) is truncated for the sake of clarity. The central Mg (magenta sphere) is coordinated in-plane by the four pyrrole nitrogens (yellows dashes) with a fifth, axial ligand (green dashes) donated by a nitrogen of His M182 (green carbons). Ligation is in the *anti* configuration (see the text). (B) Cofactor nomenclature and organization in the *Rba. sphaeroides* RC. Most of the hydrocarbon side chains of the BChl, BPhe, and ubiquinone cofactors have been removed for the sake of clarity. Carbons are colored yellow for the P BChls, cyan for the B_A/B_B BChls, salmon for the H_A/H_B BPhes, green for the Q_A/Q_B quinones, and turquoise for the carotenoid (Crt). Other atom colors are as in panel A. The route of transmembrane electron transfer is indicated by the arrows.

same side of the BChl macrocycle as the phytol chain. All four BChls of the purple bacterial RC exhibit *anti* ligation, and there is a strong bias toward *anti* ligation in photosynthetic proteins (*12*−*14*).

The purple bacterial RC was the first integral membrane protein to yield a high-resolution X-ray crystal structure (*15*, *16*). In *Rba. sphaeroides*, the RC consists of three polypeptides, termed H, L, and M, that encase four BChl *a* molecules, two bacteriopheophytin *a* (BPhe) molecules, two ubiquinones, a single photoprotective carotenoid, and a non-heme iron atom. The BChl, BPhe. and ubiquinone cofactors are arranged around an axis of pseudo-2-fold symmetry in two membrane-spanning branches (*17*−*20*) (Figure 1B). Light excitation of the RC triggers electron transfer across the membrane along the A-branch (Figure 1B, arrows) from a pair of excitonically coupled BChl molecules (P_A/P_B, denoted P) to the Q_A ubiquinone (see refs (*21*−*25*) for reviews). In the first step, an electron is passed from the lower-energy singlet excited state of P (denoted P*) to the adjacent A-branch monomeric BChl (B_A), forming the $P^+B_A^-$ radical pair with a time constant of 3−5 ps at room temperature. The electron is then passed to the A-branch BPhe (H_A), forming the $P^+H_A^-$ radical pair with a time constant of 0.5−2 ps. The second of these reactions is more rapid than the first, the result being that the $P^+B_A^-$ radical pair is difficult to detect as a discrete intermediate as the electron is passed from P* to H_A. The electron is then transferred from H_A^- to Q_A with a time constant of ∼200 ps (*21*−*25*).

All four of the BChl cofactors in the *Rba. sphaeroides* RC are pentacoordinated (*17*−*20*), with the fifth ligand donated by a His residue in the *anti* configuration (Figure 1A). If one of these His ligands is replaced with an apolar residue through site-directed mutagenesis, then a metal-free BPhe is incorporated in place of the native BChl during assembly of the complex (*26*, *27*). These experiments have demonstrated that BChl cannot be stably incorporated into the protein structure in the absence of an axial ligand. One constraint for the structure of a (B)Chl binding site in a photosynthetic protein is therefore the provision of a suitable ligand donor at a position over the center of one face of the tetrapyrrole macrocycle.

Reports of naturally occurring hexacoordinated (B)Chls in photosynthetic proteins are confined to two recent publications, one presenting spectroscopic evidence for partial hexacoordination in the *Rhodospirillum rubrum* LH1 antenna complex (*28*) and the other presenting crystallographic evidence for a hexacoordinated BChl in the Fenna−Matthews−Olson (FMO) light-harvesting protein from *Prosthecochloris aestuarii* (*29*). With the exception of these two cases, considered in more detail in the Discussion, (B)Chl cofactors in photosynthetic complexes of known structure are uniformly pentacoordinated (*3*−*11*). Thus, a second major constraint for the structure of a (B)Chl binding site in a photosynthetic protein appears to be exclusion of any groups that could donate a sixth ligand to the Mg of the tetrapyrrole on the opposite side of the macrocycle from the mandatory fifth ligand.

The biophysical consequences of introducing a sixth ligand into a protein-bound (B)Chl cofactor remain largely unexplored. However, DiMagno and co-workers have described the properties of a mutant *Rhodobacter capsulatus* RC in which Phe 181 of the L-polypeptide was altered to Lys (denoted FL181K) (*30*). This residue is located close to the center of the macrocycle of the monomeric BChl on the B-branch of cofactors (denoted B_B), on the opposite side from residue His M182 that donates the fifth ligand to the central Mg of B_B (Figure 1A). The FL181K mutation produced a change in the absorbance spectrum of the RC BChls that was consistent with hexacoordination of the B_B BChl (see below). The rate of primary charge separation, measured as the average lifetime of the P* state, was somewhat accelerated from 5.0 ps in the wild type to 4.0 ps in the mutant, an effect that may have been connected to a small increase in the midpoint potential for one-electron oxidation of P, from 492 mV in the wild type to 502 mV in the mutant (*30*). In a subsequent study on a *Rba. sphaeroides* RC with this mutation, the conclusion that a Lys at the L181 position elicits hexacoordination of B_B was supported by a partially refined X-ray crystal structure that showed the new Lys side chain at the L181 position pointing toward the central Mg of the B_B cofactor, with proposed direct coordination between the Lys side chain and the Mg atom (*31*). Such direct coordination by a strong base has not been reported in other X-ray crystal structures for (B)Chl-containing proteins. Hexacoordination also involved the Mg of the B_B cofactor adopting a more symmetrical, in-plane geometry (*31*).

In this work, the effects of a Phe to Arg mutation at the L181 position (FL181R) have been examined. A combination of steady

state spectroscopy and X-ray crystallography is used to demonstrate that this mutation also causes the B_B BChl to become hexacoordinated, and the nature of the new ligand and the effects on the detailed conformation of the B_B cofactor are discussed. The extent to which resonance Raman spectroscopy can be used to detect this shift in coordination state is also explored. Functional effects of the FL181R mutation are described, and the question of whether B_B can be returned to a pentacoordinated state by removal of the native ligand is investigated. Possible reasons why hexacoordinated (B)Chls do not appear to be present at appreciable levels in photosynthetic proteins are discussed.

EXPERIMENTAL PROCEDURES

Biological Material. All mutations were generated using the QuikChange mutagenesis procedure (Stratagene). The template was plasmid pUCXB-1, which is a derivative of pUC19 containing a 1841 bp *Xba*I−*Bam*HI restriction fragment encompassing *pufLM* (*32*). Mutagenic changes were confined to codon 181 of the *pufL* gene and/or codon 182 of the *pufM* gene and were confirmed by DNA sequencing. The mutated genes were expressed in *Rba. sphaeroides* deletion strain DD13 (*33*), using a derivative of expression vector pRKEH10D that lacks the *pufBA* genes that encode the core LH1 antenna complex (*33*). This produced transconjugant strains that had mutant RCs but lacked both the LH1 and LH2 light-harvesting complex.

Experimental material for steady state and time-resolved absorbance spectroscopy consisted of intracytoplasmic membrane fragments prepared from cells that had been grown under semiaerobic conditions in the dark, using procedures described previously (*34*). For the preparation of purified RCs for absorbance spectroscopy, resonance Raman spectroscopy, or X-ray crystallography, membrane fragments were suspended in 20 mM Tris-HCl (pH 8.0) and RCs were solubilized by the addition of NaCl to a final concentration of 100 mM and lauryl dimethylamine oxide (LDAO) to a final concentration of 1.5%. Solubilized RCs suspended in 20 mM Tris-HCl and 0.1% LDAO (pH 8.0) were purified by two sequential passes through a DE52 anion exchange column, followed by passage through Sepharose Q and Sephadex 200 columns (Pharmacia), as described in detail previously (*32*).

Assays of BChl and BPhe content were conducted on RCs that had been pelleted by overnight ultracentrifugation and dried by vacuum desiccation at room temperature for 1 h in a SpeedVac dryer (Thermo Electron). A 1 mL aliquot of a 7:2 (v:v) acetone/methanol mixture was added to the dried RCs and the pellet resuspended by ultrasonication. Debris was removed by centrifugation in a benchtop centrifuge before the absorbance spectrum of the supernatant was recorded (see the text). Assays were repeated at least three times, and values reported in the text are averages (±standard deviation)

Steady State and Time-Resolved Spectroscopy. Absorbance spectra were recorded on a Perkin-Elmer UV−vis Lamda-35 spectrophotometer. Spectra at 77 K were recorded using an Oxford Instruments DN1704 liquid nitrogen cryostat. Low-temperature resonance Raman spectra were recorded as described previously (*35*). Excitation at 799.3 nm was provided by a Krypton ion laser (Coherent Innova).

Femtosecond transient absorbance difference spectra were recorded using antenna-deficient membranes and a spectrometer that has been described in detail previously (*36*, *37*). In brief, the output of a Ti:sapphire oscillator was amplified by means of chirped pulse amplification (Alpha-1000 US, B.M. Industries) generating 1 kHz, 795 nm, 60 fs pulses. The absorption of the sample was 0.6 OD mm^{-1} at 795 nm, and typically, 20% of the RCs were excited with each pulse. The steady state absorption spectrum of the sample before and after measurements did not show any changes. Spectra were corrected for white light group velocity dispersion and the instrument response function and fitted globally with four components as described previously (*38*).

X-ray Crystallography. Trigonal crystals of the FL181R RC, space group $P3_121$, were grown by sitting drop vapor diffusion as described previously (*32*). Briefly, well solutions containing 9 mg/mL FL181R RC, 0.09% (v:v) LDAO, 3.5% (w:v) heptane-1,2,3-triol, and 0.65 M potassium phosphate (pH 8.0) were equilibrated against a reservoir solution of 1.5 M potassium phosphate. Crystals appeared within 1−2 weeks and presented as prisms of variable size. The crystals had the following unit cell dimensions: $a = b = 140.2$ Å, $c = 185.7$ Å, $\alpha = \beta = 90°$, and $\gamma = 120°$. X-ray diffraction data were collected using cryo-cooled crystals and an ADSC Quantum 4 detector, on beamline 14.1 of the Daresbury Synchrotron Facility (Warrington, U.K.). Crystals were prepared for cryocooling by being sequentially soaked in mother liquor containing increasing concentrations of ethylene glycol to give a final concentration of 30%. The crystal used for data collection diffracted to a higher-resolution limit of 2.56 Å, and diffraction data collected over the range of 44.5−2.72 Å were processed and scaled using XDS (*39*). Molecular replacement was performed using AMORE (*40*) using the coordinates of the wild-type RC as the search model (*32*). Partial refinement was performed using restrained maximum likelihood refinement in REFMAC version 5.0 (*41*). Modeling of the area surrounding the L181 residue was conducted on the basis of omit maps, with the L181 residue as Ala in the initial round of refinement. Data collection and refinement statistics are listed in Table 1.

RESULTS

Steady State Absorption Spectroscopy. Figure 2A shows the near-infrared region of the absorbance spectrum of membrane-bound wild-type and FL181R mutant RCs, recorded using intracytoplasmic membranes prepared from antenna-deficient strains of *Rba. sphaeroides* as described in Experimental Procedures. For the wild-type RC, the band with a maximum at ~756 nm can be attributed to the RC BPhes (termed the H Q_y band), the band at ~804 nm to the accessory BChls with a smaller contribution from the P BChls (termed the B Q_y band), and the band at ~868 nm to the P BChls (termed the P Q_y band). In the Q_x region, the band at ~598 nm can be attributed to all four RC BChls (these labels are shown in Figure 2B). The sloping baseline in the region between 950 and 650 nm and the marked increase in absorbance at shorter wavelengths are caused by scatter from the membrane. This scatter and absorption from other membrane components obscure the Q_x absorbance band attributable to the two RC BPhes at ~540 nm, and this region of the spectrum is not shown in Figure 2A.

The FL181R mutation produced two notable changes to this spectrum. The first was an approximately 4 nm blue shift of the maximum of the B Q_y band, consistent with a mutation near one of the accessory BChls. This was accompanied by 1−2 nm red shifts in the maxima of the P and H Q_y bands which, although small, were seen consistently in spectra of both membrane-bound and purified RCs at room temperature and 77 K. Second, the spectrum of the FL181R mutant exhibited a new small

Table 1: Crystallographic Statistics for Data Collection with the FL181R RC

Data Collection Statistics	
resolution range (Å)	44.5−2.72
outer shell (Å)	2.87−2.72
no. of unique observations	56225
redundancy	4.6 (4.4)
completeness (outer shell)	98.5 (97.8)
R_{sym} (%)[a] (outer shell)	0.09 (0.50)
mean $I/\sigma I$ (outer shell)	8.6 (2.1)
Refinement	
data range (all data with $F > 0.0$)	20.4−2.72
no. of reflections in the working set (test set)	53598 (2627)
R factor (outer shell)[b]	23.5 (27.6)
R_{free} (outer shell)[c]	34.0 (42.0)
rmsd for bonds (Å)	0.019
rmsd for angles (deg)	2.22
average B factor (Å^2)	68.3
Model	
no. of protein residues	822
no. of cofactors[d]	4 BChl, 2 BPhe, 1 Ubi, 1 Fe, 1 Spn
no. of waters	310
no. of other components[e]	1 CDL, 6 LDA, 3 HTO 1 GOL, 1 Na^+

[a] R_{sym} is defined by $\sum_h |I_h - \bar{I}_h| / \sum_h \bar{I}_h$, where I_h and $\bar{I}_h$ are the intensities of two symmetry-related reflections and $\sum_h$ is the sum over all reflections. [b] R factor is defined by $\sum ||F_o| - |F_c|| / \sum |F_o|$. [c] R_{free} was calculated with 5% of the reflections selected to be the same as in the refinement of the wild-type RC (*32*). [d] Ubi, ubiquinone; Spn, spheroidenone. [e] CDL, cardiolipin; LDA, LDAO; GOL, glycerol; HTO, heptane-1,2,3-triol.

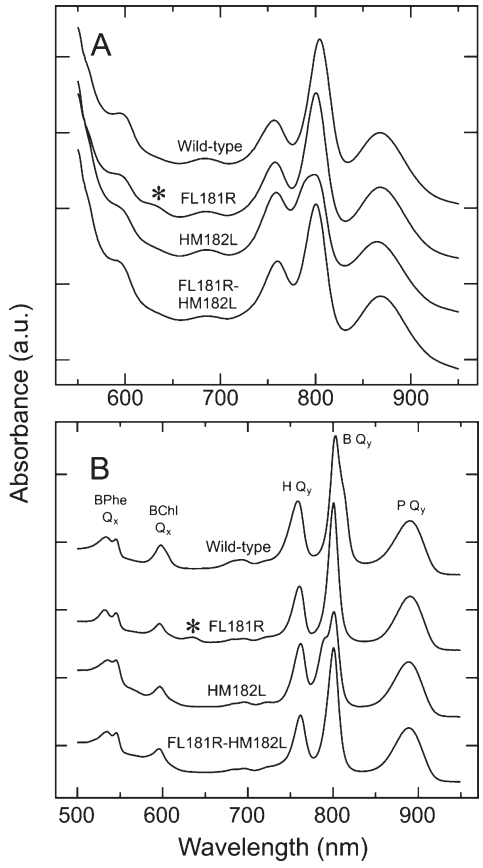

FIGURE 2: Absorbance spectra of antenna-deficient membranes and purified RCs. Panel A shows the room-temperature spectra of membrane-bound RCs. The spectra are superimposed on background scatter from the membrane which increases at shorter wavelengths and, below 600 nm, on background absorbance from other membrane components. Panel B shows the 77 K spectra of purified RCs. In both panels, the spectra have been normalized to the same amplitude of the P Q_y band and offset for the sake of comparison, and the asterisk indicates the absorbance band indicative of a hexacoordinated BChl in the FL181R single mutant RC.

absorbance band with a maximum in the region of 630−632 nm (indicated by the asterisk in Figure 2A), the possible origins of which are considered below. The appearance of this new band in the Q_x region occurred alongside a 1−2 nm blue shift of the maximum of the BChl Q_x band at 598 nm. A wild-type minus FL181R mutant difference spectrum (not shown) indicated the appearance of a component centered at 631 nm in the mutant coupled with the loss of a component centered at 600 nm in the wild type.

To examine the effects of the FL181R mutation in more detail, absorbance spectra were also recorded for purified RCs at room temperature (data not shown) and 77 K (Figure 2B). The spectral changes seen for membrane-bound FL181R RCs were preserved in the spectrum of the purified complex at room temperature (not shown), including the new absorbance band around 632 nm. The Q_x absorbance band of the two BPhes, centered at ~540 nm, was resolved in the room-temperature spectra of purified RCs, and the shape and position of this band were not affected by the FL181R mutation (not shown).

The increased resolution of the spectra of purified RCs recorded at 77 K (Figure 2B) allowed three additional observations. First, the Q_x transitions of the two BPhe cofactors were resolved as discrete bands at 545 nm for H_A and 533.5 nm for H_B in the spectrum of the wild-type RC (Figure 2B). The position of the 545 nm band was unchanged in the 77 K spectrum of purified FL181R RCs, but the maximum of the band attributed to H_B was blue-shifted to 532 nm. Second, the pronounced shoulder on the red side of the asymmetric B Q_y band in the spectrum of the wild-type RC, attributed in many studies to the B_B BChl, was not present in the spectrum of the FL181R mutant. This was not due to the absence of this component, but rather a blue shift of its absorbance maximum to produce a much sharper B Q_y band in the spectrum of the mutant (Figure 2B). Finally, the Q_x band of the RC BChls also showed a distinct change in line shape. In the spectrum of the wild-type RC, this band had a pronounced asymmetry, with a main component around 598 nm and a shoulder at ~606 nm. In the spectrum of the FL181R mutant, the main band was at approximately 596 nm but was diminished in intensity, and the shoulder at longer wavelengths was not resolved. However, a new band was observed with a maximum at 635 nm (asterisk in Figure 2B), and a difference spectrum indicated the loss of a component in the spectrum of the wild-type RC centered at 603 nm accompanied by the appearance of a new component in the spectrum of the mutant centered at 635 nm (not shown).

The principal effect of the FL181R mutation was therefore a pronounced red shift in the Q_x absorbance band of one or more BChl cofactors, and given the location and character of the mutation, a possible explanation is a change in the coordination state of the monomeric B_B BChl. A number of research groups have reported, on the basis of studies of BChl *a* in solvent, that the absorbance maximum of the Q_x band in the spectrum of hexacoordinated BChl *a* is located approximately 30−40 nm to the red of that of pentacoordinated BChl *a* (*42*−*44*). Accordingly

the ~31 nm red shift of a BChl Q_x band seen in the spectrum of the FL181R mutant is consistent with a change in the B_B BChl cofactor from penta- to hexacoordination. An effect of the mutation on the B_B BChl would also be consistent with the observed sharpening and small blue shift of the B Q_y band seen in the 77 K spectra, together with small effects on the absorbance properties of the neighboring H_B BPhe, which is also located close to the mutated Phe L181 residue.

These conclusions implied that the BChl content of the FL181R RC should be unaltered. To examine this, the bacteriochlorin cofactors were extracted from purified RCs using an acetone/methanol mixture (7:2, v:v), as described in Experimental Procedures. Absorbance spectra of the extracts were analyzed as described by van der Rest and Gingras (*45*) (data not shown), and the resulting BChl:BPhe ratios for the wild type and FL181R mutant were 1.83 ± 0.07 and 2.05 ± 0.35, respectively, consistent with a normal complement of four BChls and two BPhes in the FL181R RC.

X-ray Crystallography. The FL181R RC was crystallized in a trigonal form, as described in Experimental Procedures, and diffraction data were collected to a maximum resolution of 2.56 Å using cryo-cooled crystals and an ADSC Quantum 4 detector, on beamline 14.1 of the Daresbury Synchrotron Facility. Data collected over the range of 44.5−2.72 Å were used for the determination of the structure by molecular replacement (see Experimental Procedures), and data collection and refinement statistics are listed in Table 1. The FL181R RC exhibited good overall structural conservation, with changes in structure being confined to the immediate vicinity of the mutation site.

Figure 3A shows $2F_o - F_c$ (blue) and $F_o - F_c$ (green for positive, red for negative) electron density maps for the region around the L181 residue and the adjacent B_B BChl, with the L181 residue modeled as an Ala. The map shows a tube of unsatisfied density (green) extending from the L181 α-carbon toward the B_B Mg. This density could be modeled as an Arg side chain (Figure 3B); however, the closest approach of the Arg side chain to this Mg (via the NH1 atom) was around 3.5 Å, which would be unusually long for a ligand (see Discussion), and difference density maps highlighted unsatisfied density in the region between the Arg side chain and the Mg of B_B (not shown). After examining a number of possibilities, including different conformations of the Arg side chain, we achieved the best fit of structure to density (Figure 3B) by including a water molecule placed between the NH1 atom of Arg L181 and the Mg of B_B, with center-to-center distances of 2.11 Å (Arg to H_2O) and 1.99 Å (H_2O to Mg) in the final refined structure.

One feature of many of the BChl and Chl molecules in structurally characterized photosynthetic proteins is that the central Mg sits slightly out of the plane of the BChl ring on the side of the axial ligand, and this is the case for the Mg of the B_B BChl in the wild-type RC (Figure 1A). Given this, one possible consequence of hexacoordination might be a pulling of this Mg into the plane of the BChl, but this was not the case in the final refined structure of the FL181R RC, where this Mg appeared not to have moved to any significant extent when the structure was overlaid with that of the wild-type RC (*32*). The remainder of the structure showed no deviations from that of the wild-type RC over and above very small (<0.3 Å) shifts expected when structures at ~2.7 Å resolution are compared (where the typical coordinate error is ~0.2−0.3 Å).

Resonance Raman Spectroscopy. Resonance Raman spectroscopy can be used to provide information about the detailed

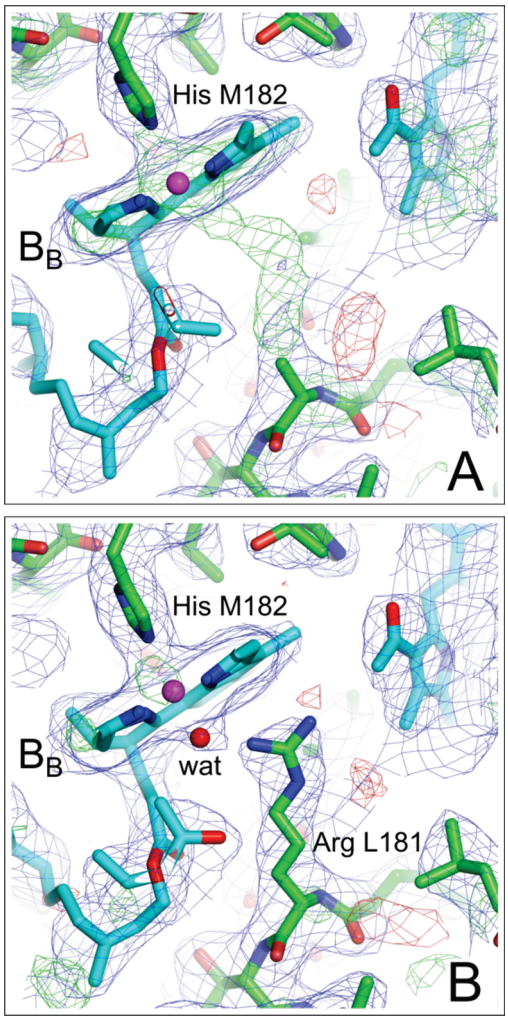

FIGURE 3: Electron density map for the region around the B_B BChl in the FL181R RC, including the native ligand donor His M182. (A) Electron density map following molecular replacement with the L181 residue modeled as an alanine. (B) Final model with a water built between the Mg of the BChl and Arg L181. Both panels show $2F_o - F_c$ electron density (blue) displayed at the 1.2σ level and $F_o - F_c$ positive electron density (green) and negative electron density (red) displayed at the 3.0σ level. Residues and cofactors are shown with green and cyan carbons, respectively, with nitrogens colored blue and oxygens red. The Mg of the B_B BChl is shown as a magenta sphere and the fitted water as a red sphere.

structure of a BChl, including the coordination number and core size. The latter is defined as the distance between the center of the molecule and the pyrrole nitrogens, and in principle, this distance could become larger if the central Mg adopts a more in-plane geometry due to a structural change such as a switch from penta- to hexacoordination (*46*, *47*). In previous resonance Raman experiments on R26.1 RCs, two excitation wavelengths were used, 800 and 810 nm, enabling near-selective excitation of B_A and B_B, respectively, and allowing the structures of the two BChls to be compared (*35*). In the case of the FL181R RC, the lack of discrete absorbance bands for B_A and B_B in the 77 K absorbance spectrum meant that such selective excitation was not possible, but nevertheless, a resonance Raman spectrum was recorded to determine if the FL181R mutation caused any discernible spectral changes consistent with hexacoordination of the B_B BChl. As with previous work, the sample of FL181R RCs was oxidized by the addition of a small amount of potassium ferricyanide prior to the measurement to minimize interference

from background fluorescence from P (see ref *35* for a discussion of this).

Figure 1A of the Supporting Information shows the overall resonance Raman scattering spectrum of FL181R RCs between 180 and 1800 cm^{-1} at 77 K, with selected regions shown on expanded scales in Figure 1B−D of the Supporting Information. A full list of the frequencies of bands observed in the resonance Raman scattering spectrum of the FL181R mutant and their assignments are listed in Table 1 of the Supporting Information, and the main differences between the data sets obtained for the FL181R and R26.1 RCs are listed in Table 2 of the Supporting Information. There was good agreement between the two data sets, confirming the result from X-ray crystallography that the FL181R mutation did not bring about any large-scale perturbation of the conformation of the B_B BChl or its protein surroundings.

A previous study performed on BChl *a* and metal-substituted Zn-, Ni-, Cu-, and Co-BPhe *a* identified a set of modes (denoted R1−R6) that are sensitive to core size and the coordination number of the central Mg (*46*). These R1−R6 modes are of obvious relevance to this study and are listed in Table 2 of the Supporting Information. The R1 methine bridge stretching mode has the greatest sensitivity to coordination state and is found at 1609 cm^{-1} for pentacoordinate BChl *a* in Et_2O and at 1595 cm^{-1} for hexacoordinate BChl *a* in THF (*46*). In the spectrum of the FL181R RC, the R1 mode was at 1611 cm^{-1}, similar to the R1 modes at 1610 cm^{-1} for both B_A and B_B in the R26.1 RC (*35*). However, this was expected as the R1 mode of B_A should be located at this position in the composite spectrum of the FL181R complex. The detection of a downshifted B_B mode around 1585 cm^{-1}, expected for a hexacoordinated B_B (*46*), was complicated by the presence of a mode at this position in the spectrum of both B_A and B_B (*35*). Therefore, it was not possible to detect the change from penta- to hexacoordination through the R1 mode. Previous work has shown that the remaining R modes have a much smaller sensitivity (< 4 cm^{-1}) to coordination number (*46*), and the difference between their positions in the spectrum of the FL181R RC and that of B_B in the R26.1 RC (*35*) was no greater than 2 cm^{-1}, which is on the order of the accuracy of the measurement.

In the low-frequency region between 200 and 400 cm^{-1}, the spectra of B_A and B_B in the R26.1 RC contain a number of modes that involve motion of the Mg atom, at 187, 329, 357, and 393 cm^{-1} for B_A and 185, 335, 353, and 391 cm^{-1} for B_B. In the spectrum of the FL181R RC, these modes were at 185, 337, 359, and 392 cm^{-1}, with the second and third of these being at frequencies rather higher than what would be expected given the composite nature of the FL181R spectrum. Therefore, this gave some indication of a change in the environment of the Mg of one of the accessory BChls in the FL181R RC. Finally, shifts in two other bands are of note. The δCNC mode situated at 435 cm^{-1} for both B_A and B_B in the R26.1 RC was shifted to 437 cm^{-1} in the composite spectrum of the FL181R mutant, and the band assigned to the νC_bC_b, s $\nu C_aC_m(\gamma)$, νCN(III) modes at 1521 cm^{-1} for B_A and 1519 cm^{-1} for B_B in the R26.1 RC was shifted to 1524 cm^{-1} in the FL181R mutant. Again, in both cases, the difference would be consistent with an upshift of the mode for the B_B BChl in the FL181R mutant of several wavenumbers.

Femtosecond Absorbance Difference Spectroscopy. Ultrafast transient absorbance difference spectroscopy was used to determine whether the FL181R mutation had any effect on the rate of A-branch photochemical charge separation. Absorbance difference spectra were recorded at varying time intervals after

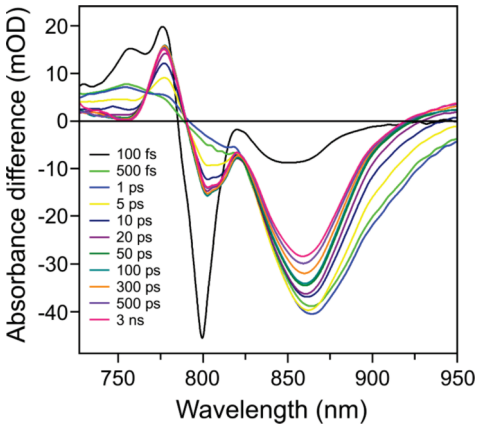

FIGURE 4: Transient absorbance difference spectra obtained at various times after excitation of membrane-bound FL181R RCs with a 60 fs excitation pulse centered at 795 nm.

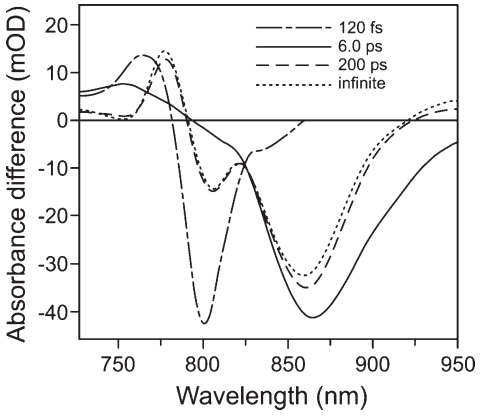

FIGURE 5: Species-associated absorbance difference spectra for the FL181R RC calculated using an irreversible sequential model with four components.

exposure of membrane-bound FL181R RCs to a 795 nm excitation pulse, with a maximum delay time of 4 ns, as described in Experimental Procedures. Experiments were conducted at room temperature, the 795 nm pulse exciting both B_A and B_B. Representative spectra recorded at several delay times are shown in Figure 4. Excitation caused a bleach around 800 nm at early delay times [100 fs spectrum (Figure 4)], and subsequent rapid excitation transfer from the monomeric BChls to the P BChl dimer caused a bleaching of the P band around 870 nm, concomitant with a loss of the bleach at 800 nm [500 fs spectrum (Figure 4)]. Stimulated emission on the red side of the bleach of the 870 nm P band was maximal at ~1 ps and subsequently decayed as the P* state decayed through electron transfer [1 ps spectrum vs 50 ps spectrum (Figure 4)]. This spectral evolution was similar to that obtained previously for wild-type RCs, with the exception that there was an ~25% decrease in the bleach of the P Q_y band at 3 ns compared to that at 5 ps. Possible origins of this feature are considered in the Discussion.

A global analysis of the data was conducted using an irreversible sequential model (i.e., 1 → 2 → 3 →). Four spectrally and temporally distinct components were needed to describe the data, and the species-associated difference spectra (SADS) of these components are shown in Figure 5. The first component was attributed to the short-lived excited states of the accessory BChls (B*), with a lifetime of 120 fs (Figure 5). This evolved into a state with a spectrum that was characteristic of P*, with a lifetime of

6.0 ps (Figure 5). This lifetime was a little longer than the lifetime of 4.5−4.8 ps previously described for membrane-bound wild-type RCs (*48*, *49*). This longer lifetime could indicate a slowing of the $P^* \rightarrow P^+H_A^-$ reaction, perhaps due to a subtle change in the properties of P, or could indicate a change in the relative influence of an alternative route for P* decay, such as charge separation to the B-branch, for example, with no change in the transfer time for the $P^* \rightarrow P^+H_A^-$ reaction. In addition, given that it has been shown that electron transfer can also be driven by B_A* in wild-type RCs (*50*), it is also possible that there was a contribution of a small amount of $P^+B_A^-$ and/or $B_A^+H_A^-$ to the 6.0 ps spectrum in Figure 5. The third state revealed by the analysis was assigned to $P^+H_A^-$ [200 ps spectrum (Figure 5)]. This state had a spectrum that was similar to that determined previously for the membrane-bound wild-type RC (*49*), and it decayed with a lifetime of 200 ps, which was the same as that associated with the $P^+H_A^- \rightarrow P^+Q_A^-$ transfer time in the membrane-bound wild-type RC [175−210 ps (*48*, *49*)]. The final state had the spectral features characteristic of $P^+Q_A^-$ and had a lifetime that was infinite on the time scale of the measurement.

Effects of Removal of the Native Ligand Donated by His M182. Having established that introduction of an Arg residue at the L181 position introduces a second axial ligand to the B_B BChl, we were also interested in whether this BChl could be returned to a pentacoordinated state by removal of the native axial ligand donated by His M182. It has been reported previously that mutation of His M182 to Leu causes a BPhe to be assembled in the RC at the B_B position, and the absorbance spectra of such a single HM182L mutant are shown in Figure 2. In the room-temperature spectrum of membrane-bound HM182L RCs, this BChl to BPhe substitution was characterized mainly by a decrease in the relative intensity of the B Q_y band and a broadening of the blue side of this band (Figure 2A). In purified RCs at 77 K (Figure 2B), this spectral change was resolved as a loss of the shoulder at ~814 nm in the spectrum of the wild-type RC, attributed to the B_B BChl, and the appearance of a new absorbance band at ~791 nm consistent with the presence of a new BPhe at the B_B position. In support of this conclusion, in the Q_x region there was a decrease in the relative intensity of the BChl Q_x band and a change in the shape of the BPhe Q_x bands, the maximum of the shorter wavelength band shifting from 533.5 nm in the wild type to 536 nm in the HM182L RC (and with a larger red shift of the composite band at room temperature). In addition, analysis of acetone/methanol extracts of the HM182L RC yielded a BChl:BPhe ratio of 1.28 ± 0.03, significantly lower than values obtained for the wild-type RC and consistent with replacement of one BChl with a BPhe in this mutant. The changes in the spectrum of the HM182L RC determined in this study showed good agreement with changes described previously for this mutant (*51*).

The FL181R mutation was combined with the HM182L change, and the equivalent spectra of the resulting double mutant are also shown in Figure 2. The room-temperature spectrum of the membrane-bound double mutant FL181R-HM182L RC (Figure 2A) was similar to that of the FL181R single mutant, with the notable exception that the band at 632 nm was absent, but was markedly dissimilar to the spectrum of the HM182L single mutant. The same conclusions could be drawn from spectra of purified RCs recorded at 77 K (Figure 2B). The lack of the spectral signatures of an additional BPhe or a hexacoordinated BChl in the spectra of the double mutant FL181R-HM182L RC indicated that this complex had assembled with a pentacoordinated BChl. However, the influence of the non-native Arg residue at the L181 position in the double mutant was still manifest as (1) a 3−4 nm red shift of the H Q_y band and a smaller (1 nm) red shift of the H_B Q_x band at 77 K and (2) a 2−4 nm blue shift of the B Q_y band and a 1−3 nm red shift of the BChl Q_x band. These small shifts indicate an influence of the new Arg residue on the adjacent B_B BChl and H_B BPhe. The precise basis of the sole axial ligand donated to the B_B BChl in the FL181R-HM182L double mutant was not pursued, but it was presumably similar to that described above for the single FL181R mutant. Analysis of acetone/methanol extracts of the FL181R-HM182L RC gave a BChl:BPhe ratio of 1.88 ± 0.24, similar to the values obtained for the wild-type and FL181R RCs (see above) and consistent with the presence of BChl at the B_B position, rather than the BPhe seen in the HM182L single mutant.

DISCUSSION

Changes in Protein Structure Precipitated by the FL181R Mutation. As explained above, data from steady state absorbance spectroscopy and X-ray crystallography demonstrated that mutation of residue Phe L181 to Arg results in hexacoordination of the B_B BChl. Examination of electron density maps obtained for the FL181R mutant showed an elongated feature consistent with the substitution of Phe with Arg. The modeled position of this Arg placed the NH1 atom in the vicinity of the central Mg of the B_B macrocycle, but two pieces of evidence suggested that the sixth ligand donated to this Mg does not arise directly from the Arg side chain. First, difference electron density maps suggested the presence of an additional small molecule in the region adjacent to the Arg and the Mg of B_B. Second, the center-to-center distance between this Mg and the NH1 atom of Arg L181 was ~3.50 Å, which is considerably longer than the distances typical for a BChl or Chl axial ligand.

To illustrate this second point, examination of the X-ray structure of the FL181R RC showed that the average N-to-Mg distance for the His ligands of the four BChl cofactors was 2.32 Å, the longest being 2.44 Å. In the structure of the wild-type RC used for molecular replacement (*32*), the equivalent distances are 2.46 Å (average) and 2.58 Å (longest). In Photosystem I, which contains 96 Chls liganded by a variety of donors (*8*), the average ligand donor-to-Mg distance is 2.30 Å, with only five Chls having a ligand distance of more than 2.5 Å and the longest being 2.77 Å. In LHCII, which has 14 Chls per monomer (*10*), no ligand distance is longer than 2.27 Å. A distance of 3.50 Å would therefore clearly be unusually long in light of data on more than 100 structurally characterized pentacoordinated BChls or Chls. It is also worth commenting that nitrogen ligands are confined to the side chain of His in the fully refined structures that have been deposited in the Protein Data Bank to date, with no examples of direct ligation by an Arg or Lys side chain.

The best match of the structural model to the electron density was obtained with a water molecule placed between the NH1 atom of Arg L181 and the Mg of B_B (Figure 3B). The distance from this water ligand to the Mg (1.99 Å) is in the range of values for the shortest ligands donated by water molecules in determined X-ray structures. Six of the Chls in Photosystem I liganded by a water have a Mg−O distance between 2.06 and 1.95 Å, and three of the water-liganded Chls in LHCII have a Mg−O distance between 2.06 and 1.87 Å. Thus, the arrangement of ligands in the FL181R structure is consistent with other cofactors liganded by water.

The details of hexacoordination in the FL181R mutant are somewhat different from those reported by Morris and coworkers for a Lys mutation at this residue (*31*). A partially refined structure at 2.9 Å resolution was determined for the FL181K mutant, showing direct ligation of the Mg of B_B by the Lys side chain, with "movement of the Mg^{2+} atom to a position in the plane of the macrocycle or slightly below the plane towards the L181 lysine" (*31*). The possibility of ligation by an intervening water was specifically excluded in the case of the FL181K complex, and therefore, the chemical identity of the ligand donor is different in the FL181R and FL181K RCs. With regard to the position of the Mg atom, although hexacoordination might be expected to pull the Mg of B_B into the plane of the macrocycle, making the structure more symmetrical, this was not the case in this study. Comparison of the structure of the FL181R RC with that of the wild-type complex, which is at a comparable resolution of 2.6 Å (*32*), showed no significant change in the position of the B_B Mg or ligating His M182 side chain relative to the BChl macrocycle. It is possible that the requirement of accommodating both the bulky Arg side chain and the ligating water in the FL181R RC meant that such an in-plane movement was precluded in the FL181R, and that such movement does not necessarily occur in response to hexacoordination.

We also investigated whether the new Arg−water structure could act as a sole coordinating ligand during assembly of the RC, through a double mutant in which the native ligand was removed by mutation of His M182 to Leu. The resulting RC had an absorbance spectrum and pigment composition consistent with the presence of a pentacoordinated BChl at the B_B position. The simplest interpretation of this result is that the Arg−water structure is indeed capable of providing a sole ligand to a pentacoordinated BChl, although the details of this will require confirmation through X-ray crystallography in future work.

Spectroscopic Consequences of Hexacoordination of B_B. Hexacoordination of B_B in the FL181R RC caused a red shift of the Q_x absorbance band of B_B from around 606 to 635 nm at 77 K, and a blue shift of its Q_y absorbance band to a position where, at 77 K, it overlapped with the Q_y absorbance of B_A, giving rise to a single, sharp band centered at 803.5 nm. The magnitude and direction of these changes were consistent with findings with penta- and hexacoordinated BChl *a* in solvent (*42*−*44*). There was also some evidence from resonance Raman spectroscopy of small changes to vibrational modes associated with the macrocycle and central Mg. However, the Raman analysis was complicated by an inability to selectively excite the hexacoordinated B_B in the Q_y region, and in particular, it was not possible to confirm the introduction of the sixth ligand using the so-called R1 vibrational mode because of the composite nature of the Raman spectrum of the FL181R mutant.

As outlined above, a Phe to Lys mutation at the L181 position has been reported also to cause hexacoordination of the B_B BChl in both *Rba. capsulatus* (*30*, *31*) and *Rba. sphaeroides* (*31*). Room-temperature spectra have been reported for both FL181K RCs, while a 4 K spectrum has been reported for the *Rba. capsulatus* RC. The shifts in band position seen in the room-temperature and 77 K absorbance spectra of the FL181R RC obtained in this work were broadly similar to those reported previously for the FL181K RC. At room temperature, the *Rba. sphaeroides* FL181K RC exhibited a new absorbance band characteristic of a hexacoordinated BChl at ~632 nm (~631 nm in this work) and a 3−4 nm blue shift of the B Q_y band. At 4 K, the *Rba. capsulatus* FL181K RC had a new absorbance band at ~634 nm, compared with that at 632 nm for the *Rba. sphaeroides* complex at 77 K in this work, and the spectra of both mutants also both exhibited a small blue shift of the Q_x band of the adjacent H_B BPhe. Thus, there was good agreement between spectral changes reported previously for the Phe to Lys mutation at the L181 position of the RC and those obtained in this work for the Phe to Arg mutation. This suggests that these changes are principally attributable to the change in coordination state of the B_B cofactor, rather than the chemical identity of the species providing the sixth ligand.

In terms of function, hexacoordination of B_B through the FL181R mutation had an only modest effect on light-driven electron transfer in the RC. The main effect observed was a small increase in the lifetime of P* from ~4.8 to ~6 ps which could have a number of causes, the most likely of which would be a small change in the properties of the adjacent P dimer. The effect was somewhat different from that seen in the *Rba. capsulatus* FL181K RC, where the average P* lifetime decreased from 5 ps in the wild type to 4 ps in the mutant, this being associated with an ~10 mV increase in the midpoint potential for oxidation of the P dimer (*31*).

A feature of the time-resolved absorbance difference spectra shown in Figure 4 was an ~25% decrease in the bleach of the P Q_y band at 3 ns compared to 5 ps. The origins of this feature were uncertain, but a possible source could be a decrease in the yield of $P^+Q_A^-$. Such spectral features have been reported previously, principally in RCs with mutations that affect the properties of H_A and/or Q_A. An example is the so-called LM214H mutant of *Rba. sphaeroides* in which the BPhe at the H_A position is replaced with BChl due to a Leu to His mutation at the M214 position (*52*); in this RC, the yield of $P^+Q_A^-$ is reduced to 60% due to slowed electron transfer to Q_A^- coupled with an accelerated rate of decay of $P^+H_A^-$ to the ground state (*52*). However, in this case, scrutiny of the X-ray crystal structure of the FL181R RC and associated electron density in the region of the Q_A quinone and adjacent H_A BPhe gave no indication of a change in the structure of the protein in this region that might affect the electron transfer properties of H_A or Q_A or decrease in the occupancy of the Q_A site. The high degree of structural conservation away from the immediate vicinity of the B_B BChl in the FL181R RC seems at odds with a possible decrease in the yield of $P^+Q_A^-$ caused by this mutation, and this issue is the subject of ongoing investigations.

Another potential effect of hexacoordination of the B_B BChl could be a change in the yield of B-branch electron transfer, and indeed, it has been reported that the FL181K mutation causes a decrease in the yield of this process when combined with mutations that impair A-branch transfer (see ref 63 in ref *31*). In previous work from our laboratories, we have assayed the effects of mutations on the yield of B-branch electron transfer through picosecond (*37*) or millisecond (*37*, *53*) transient absorbance spectroscopy in a background containing the Ala M260 to Trp (AM260W) and Leu M214 to His (LM214H) double change. The AM260W mutation causes steric exclusion of the Q_A ubiquinone (*54*), while the LM214H mutation lowers the efficiency of A-branch charge separation (see ref *52*). A triple FL181R-AM260W-LM214H mutant was constructed with a view of conducting such an analysis, but unfortunately, this RC did not assemble in the membrane.

Do Hexacoordinated (B)Chls Occur in Vivo? The growing body of high-resolution structural data on Chl- and BChl-containing proteins seems to suggest that hexacoordination is avoided in photosynthetic pigment proteins. However, two reports have questioned whether this is an absolute rule. In the

first, Fiedor conducted deconvolution on the BChl Q_x absorbance band in purified or reconstituted LH1 antenna complexes from *Rsp. rubrum* and found that accurate fitting required a major component (76−81%) at ~589 nm and a minor component (24−19%) to account for a shoulder with a maximum at 601−611 nm (*28*). This minor component was interpreted as arising from a minor population of hexacoordinated BChls, the structural flexibility of the LH1 complex being responsible for the heterogeneity in coordination state.

Although it is possible that this red-shifted population may have been due to hexacoordination, it is noticeable that the absorbance maximum of the BChl Q_x band of this minor population was between 601 and 611 nm, well to the blue of the absorbance band for hexacoordinated BChl *a* seen in this study and reported previously (*30*, *31*, *42*−*44*). In addition, the difference in absorbance maximum between the penta- and hexacoordinated populations was between 12 and 22 nm, a smaller difference than the ~30 nm red shift attributed to hexacoordination in this study, and reported in previous work (*30*, *31*, *42*−*44*).

A complicating issue is the fact that the position of the Q_x transition is sensitive to variations in structure other than hexacoordination, and shifts of the BChl Q_x transitions have been described in a number of reports about the spectroscopic consequences of mutagenesis, albeit mainly in spectra recorded at 77 K (see refs *30* and *55*−*57* for examples). As an illustration, in previous work from our laboratories, we showed that whereas the 77 K absorbance spectrum of the wild-type RC had an asymmetric BChl Q_x band at 597 nm with a shoulder at ~605 nm, the equivalent spectrum for a GM203D mutant contained two discrete components at 604 and 590 nm and that of a GM203L mutant had two components at 604 and 588 nm (*55*). The simplest interpretation of this is a 7−9 nm blue shift of a component present at 597 nm in the wild-type RC. In this case, it is known from crystallographic data that neither mutation affects the coordination state of the RC BChls but instead removes a hydrogen bond interaction between the keto C═O group of the B_A BChl and the surrounding protein (*55*). Furthermore, in a study of the spectroscopic consequences of 11 single or double mutations at the symmetrical M210 and L181 positions (*30*), DiMagno and co-workers found that a single BChl Q_x band at 597 nm in the 4 K absorbance spectrum of the wild-type RC was replaced with two components located at 587−593 and 597−602 nm in the spectra of the mutants, with a splitting between the two absorbance maxima between 8 and 17 nm. The one exception to this was a FL181K single mutant, which had an additional discrete band at 634 nm [attributable to a hexacoordinated B_B (see above)]. Given these observations, it seems possible that 10−20 nm variations in the energy of the Q_x transition of a BChl such as those analyzed by Fiedor (*28*) could in principle arise from variation in the details of the protein structure other than the coordination state of the central Mg.

The second report of hexacoordination in a native complex concerns the X-ray crystal structure of the FMO protein, a water-soluble component of the antenna of green sulfur bacteria that connects the main chlorosome antenna to the RC. This protein has a trimeric architecture, each monomer binding seven molecules of BChl *a*, and can be isolated from different species as one of two types that can be distinguished spectroscopically at 77 K. Recently determined X-ray crystal structures for the FMO protein from *Chlorobaculum tepidum* (*29*, *58*) and *Ptc. aestuarii* 2K (*29*) have revealed the presence of an eighth BChl located in a surface cleft of the protein, the location and orientation of this BChl indicating a possible role as a conduit for the transfer of energy from the chlorosome to the FMO pigment system. In *Cbl. tepidum*, which has a type 2 FMO complex, the additional eighth BChl is pentacoordinate, whereas in *Ptc. aestuarii* 2K, which has a type 1 complex, this BChl is hexacoordinate (*29*). In the latter, the fifth ligand that is common to both complexes, donated by a backbone carbonyl oxygen, is augmented by a sixth ligand donated by the side chain oxygen of a serine (residue 123) present in a second monomer in the trimer. The hexacoordinated BChl is therefore bound at the interface of two monomers, with an axial ligand donated by each. In *Cbl. tepidum*, residue Ser 123 is replaced with Ala, precluding hexacoordination by this residue.

Tronrud and co-workers (*29*) have attempted to correlate the changes in sequence associated with hexacoordination of the eighth BChl with the two types of 77 K spectrum known for the FMO protein and shown that the presence of the residue that provides the second ligand can indeed be correlated with a type 1 complex. However, in the context of our report, and previous investigations of the effect of hexacoordination on the absorbance spectrum of BChl *a* (*30*, *31*, *42*−*44*), it is worth noting that the main differences in spectra between type 1 and type 2 FMO complexes involve the relative amplitudes of bands in the Q_y region, with only very small changes in line shape of the BChl Q_x band. This is difficult to reconcile with what is known from this study, and previous work, about the relatively pronounced effects of hexacoordination on the BChl Q_x band, and much smaller effects expected for the Q_y bands. In particular, the 77 K spectrum of the type 1 complex from *Ptc. aestuarii* 2K does not contain a discrete band that is significantly (> 30 nm) red-shifted from the main BChl Q_x band, unlike the spectrum of the FL181R RC described above.

An additional point to note from the work of Tronrud and co-workers (*29*), and also a previous report on the *Cbl. tepidum* FMO protein (*58*), is that the eighth BChl was present at a substoichiometric occupancy in the crystals used to collect diffraction data (estimated at ~34% in the case of the *Ptc. aestuarii* 2K complex). This raises questions concerning whether this site is fully occupied in the complex in vivo, and the physiological significance, if any, of the hexacoordination seen in certain species (see ref *29* for a discussion). A low occupancy of this site could explain the lack of an obvious spectral signature of a hexacoordinated BChl in the Q_x region of the 77 K spectrum of the *Ptc. aestuarii* 2K FMO complex but could not explain the very obvious spectral changes in the Q_y region that have been correlated with the protein sequence differences that facilitate hexacoordination.

Why Are All Structurally Characterized BChls Pentacoordinated? The data described in the Results, and those of Morris and co-workers (*31*) reported previously, show that it is possible to hexacoordinate a protein-bound BChl without there being drastic effects on the structure of the surrounding protein or the main Q_y absorbance band of the BChl. Nevertheless, with the exception of the low-occupancy FMO BChl described in the previous section, all of the structurally characterized BChls and Chls reported to date appear to be pentacoordinated, which places a significant limitation on the structure of the surrounding protein scaffold and possible cofactor−cofactor geometries (the latter point stems from the fact that in aggregates of BChl the keto or acetyl groups of one BChl can act as a ligand donor to the Mg of a neighboring BChl). Hexacoordination seems to be avoided, although, as outlined in the previous section, this may

not be an absolute rule. To avoid hexacoordination, each (B)Chl binding pocket in these protein−cofactor systems has an asymmetric structure, with one ligand-donating side and a side devoid of any potential ligand donors, even in proteins such as PS-I and LHC-II that contain large numbers of relatively densely packed (B)Chl cofactors. Why hexacoordinated BChls are avoided in these proteins remains unclear as, from the point of view of light harvesting, which is the principal function of most protein-bound (B)Chls, hexacoordination has only modest effects on the Q_y absorbance of these cofactors, as is apparent from Figure 2. The principal effect is rather a decrease in the energy of the Q_x transition of the hexacoordinated BChl, but there is no particular reason to believe that overall light harvesting and energy transfer would be adversely affected by changing the energy of the Q_x transition relative to the Soret and Q_y transitions.

A possible reason why hexacoordination is avoided in photosynthetic systems concerns the redox properties of BChl. Although most studies of the effects of hexacoordination have focused on the optical properties of BChl and related pigments, some study of consequences for both oxidation and reduction of BChl has also been pursued (*59*, *60*). Noy and coworkers (*60*) have reported that a shift from penta- to hexacoordination is associated with a decrease of approximately 140 mV in the midpoint potential for single-electron reduction of BChl, and an increase of approximately 90 mV in the midpoint potential for single-electron oxidation. It is therefore conceivable that the consistent pentacoordination seen in light-harvesting systems is required to ensure approximate uniformity of the redox properties of the constituent BChls, to prevent the occurrence of unwanted charge separation reactions that could interfere with productive energy or electron transfer processes.

Unfortunately, it is not possible to assay the redox properties of the B_B BChl in the *Rba. sphaeroides* RC, so the actual impact of the FL181R mutation on parameters such as the free energy of the $P^+B_B^-$ state is not known. However, it is interesting to note that an equivalent FL181K mutation, which also induces hexacoordination of B_B, is reported to cause a decrease in the yield of B-branch electron transfer when combined with mutations that impair A-branch transfer (*31*). This effect is consistent with a shift in the midpoint potential of the B_B/B_B^- couple to more negative values, which would be expected to increase the free energy of the $P^+B_B^-$ intermediate and make B-branch electron transfer less accessible.

To close, it remains to be established whether the introduction of hexacoordinated BChls or Chls into a light-harvesting system would cause unwanted charge separation reactions or impair the efficiency of light harvesting and energy transfer in other ways. However, the high-resolution information now available for proteins such as LHC-II, PS-I, and PS-II should allow this to be tested, using the type of approach described for B_B in the purple bacterial RC.

SUPPORTING INFORMATION AVAILABLE

Figure showing the resonance Raman spectrum acquired for ferricyanide-treated FL181R RCs at 77 K excited at 799.3 nm, a table of maxima of main bands observed in this spectrum, and a table showing main differences in band maxima observed in resonance Raman spectra from ferricyanide-treated FL181R and R26 RCs at 77 K. This material is available free of charge via the Internet at http://pubs.acs.org.

REFERENCES

1. Blankenship, R. E. (2002) Molecular Mechanisms of Photosynthesis, pp 42−55, Blackwell Science Ltd., Oxford, U.K.
2. Senge, M. O., and Smith, K. M. (1995) Biosynthesis and structures of the bacteriochlorophylls. In Anoxygenic Photosynthetic Bacteria (Blankenship, R. E., Madigan, M. T., and Bauer, C. E., Eds.) pp 137−151, Kluwer Academic Publishers, Dordrecht, The Netherlands.
3. Fenna, R. E., and Matthews, B. W. (1975) Chlorophyll arrangement in a bacteriochlorophyll protein from *Chlorobium limicola*. *Nature 258*, 573–577.
4. Deisenhofer, J., Epp, O., Sinning, I., and Michel, H. (1995) Crystallographic refinement at 2.3-angstrom resolution and refined model of the photosynthetic reaction-center from *Rhodopseudomonas viridis*. *J. Mol. Biol. 246*, 429–457.
5. McDermott, G., Prince, S. M., Freer, A. A., Hawthornthwaite-Lawless, A., Papiz, M. Z., Cogdell, R. J., and Isaacs, N. W. (1995) Crystal structure of an integral membrane light-harvesting complex from photosynthetic bacteria. *Nature 374*, 517–521.
6. Hofmann, E., Wrench, P. M., Sharples, F. P., Hiller, R. G., Welte, W., and Diederichs, K. (1996) Structural basis of light harvesting by carotenoids: Peridinin-chlorophyll-protein from *Amphidinium carterae*. *Science 272*, 1788–1791.
7. Koepke, J., Hu, X. C., Muenke, C., Schulten, K., and Michel, H. (1996) The crystal structure of the light-harvesting complex II (B800−850) from *Rhodospirillum molischianum*. *Structure 4*, 581–597.
8. Jordan, P., Fromme, P., Witt, H. T., Klukas, O., Saenger, W., and Krauss, N. (2001) Three-dimensional structure of cyanobacterial photosystem I at 2.5 Å resolution. *Nature 411*, 909–917.
9. Ferreira, K. N., Iverson, T. M., Maghlaoui, K., Barber, J., and Iwata, S. (2004) Architecture of the photosynthetic oxygen-evolving center. *Science 303*, 1831–1838.
10. Liu, Z. F., Yan, H. C., Wang, K. B., Kuang, T. Y., Zhang, J. P., Gui, L. L., An, X. M., and Chang, W. R. (2004) Crystal structure of spinach major light-harvesting complex at 2.72 Å resolution. *Nature 428*, 287–292.
11. Guskov, A., Kern, J., Gabdulkhakov, A., Broser, M., Zouni, A., and Saenger, W. (2009) Cyanobacterial photosystem II at 2.9-angstrom resolution and the role of quinones, lipids, channels and chloride. *Nat. Struct. Mol. Biol. 16*, 334–342.
12. Balaban, T. S., Fromme, P., Holzwarth, A. R., Krauss, N., and Prokhorenko, V. I. (2002) Relevance of the diastereotopic ligation of magnesium atoms of chlorophylls in Photosystem I. *Biochim. Biophys. Acta 1556*, 197–207.
13. Oba, T., and Tamiaki, H. (2002) Which side of the π-macrocycle plane of (bacterio)chlorophylls is favored for binding of the fifth ligand? *Photosynth. Res. 74*, 1–10.
14. Balaban, T. S., Braun, P., Hattig, C., Hellweg, A., Kern, J., Saenger, W., and Zouni, A. (2009) Preferential pathways for light-trapping involving β-ligated chlorophylls. *Biochim. Biophys. Acta 1787*, 1254–1265.
15. Deisenhofer, J., Epp, O., Miki, K., Huber, R., and Michel, H. (1984) X-ray structure analysis of a membrane protein complex: Electron-density map at 3 Å resolution and a model of the chromophores of the photosynthetic reaction center from *Rhodopseudomonas viridis*. *J. Mol. Biol. 180*, 385–398.
16. Deisenhofer, J., Epp, O., Miki, K., Huber, R., and Michel, H. (1985) Structure of the protein subunits in the photosynthetic reaction center of *Rhodopseudomonas viridis* at 3 Å resolution. *Nature 318*, 618–624.
17. Allen, J. P., Feher, G., Yeates, T. O., Komiya, H., and Rees, D. C. (1987) Structure of the reaction center from *Rhodobacter sphaeroides* R-26: The cofactors. *Proc. Natl. Acad. Sci. U.S.A. 84*, 5730–5734.
18. Chang, C.-H., El-Kabbani, O., Tiede, D., Norris, J., and Schiffer, M. (1991) Structure of the membrane-bound protein photosynthetic reaction center from *Rhodobacter sphaeroides*. *Biochemistry 30*, 5352–5360.
19. Ermler, U., Fritzsch, G., Buchanan, S. K., and Michel, H. (1994) Structure of the photosynthetic reaction center from *Rhodobacter sphaeroides* at 2.65-angstrom resolution: Cofactors and protein-cofactor interactions. *Structure 2*, 925–936.
20. Ermler, U., Michel, H., and Schiffer, M. (1994) Structure and function of the photosynthetic reaction center from *Rhodobacter sphaeroides*. *J. Bioenerg. Biomembr. 26*, 5–15.
21. Parson, W. W. (1991) Reaction centers. In Chlorophylls (Scheer, H., Ed.) pp 1153−1180, CRC Press, Boca Raton, FL.
22. Woodbury, N. W., and Allen, J. P. (1995) The pathway, kinetics and thermodynamics of electron transfer in wild type and mutant bacterial reaction centers of purple nonsulfur bacteria. In Anoxygenic

Photosynthetic Bacteria (Blankenship, R. E., Madigan, M. T., and Bauer, C. E., Eds.) pp 527−557, Kluwer Academic Publishers, Dordrecht, The Netherlands.
23. Parson, W. W. (1996) Photosynthetic bacterial reaction centers. In Protein Electron Transfer (Bendall, D. S., Ed.) pp 125−160, BIOS Scientific Publishers, Oxford, U.K.
24. Hoff, A. J., and Deisenhofer, J. (1997) Photophysics of photosynthesis: Structure and spectroscopy of reaction centres of purple bacteria. *Phys. Rep. 287*, 2–247.
25. van Brederode, M. E., and Jones, M. R. (2000) Reaction centres of purple bacteria. In Enzyme-Catalysed Electron and Radical Transfer (Scrutton, N. S., and Holzenburg, A., Eds.) pp 621−676, Kluwer Academic/Plenum Publishers, New York.
26. Bylina, E. J., and Youvan, D. C. (1988) Directed mutations affecting spectroscopic and electron transfer properties of the primary donor in the photosynthetic reaction center. *Proc. Natl. Acad. Sci. U.S.A. 85*, 7226–7230.
27. Katilius, E., Turanchik, T., Lin, S., Taguchi, A. K. W., and Woodbury, N. W. (1999) B-side electron transfer in a *Rhodobacter sphaeroides* reaction center mutant in which the B-side monomer bacteriochlorophyll is replaced with bacteriopheophytin. *J. Phys. Chem. B 103*, 7386–7389.
28. Fiedor, L. (2006) Hexacoordination of bacteriochlorophyll in photosynthetic antenna LH1. *Biochemistry 45*, 1910–1918.
29. Tronrud, D. E., Wen, J., Gay, L., and Blankenship, R. E. (2009) The structural basis for the difference in absorbance spectra for the FMO antenna protein from various green sulfur bacteria. *Photosynth. Res. 100*, 79–87.
30. DiMagno, T. J., Laible, P. D., Reddy, N. R., Small, G. J., Norris, J. R., Schiffer, M., and Hanson, D. K. (1998) Protein-chromophore interactions: Spectral shifts report the consequences of mutations in the bacterial photosynthetic reaction center. *Spectrochim. Acta, Part A 54*, 1247–1267.
31. Morris, Z. S., Hanson, D. K., Pokkuluri, P. R., Mets, D. G., Hata, A. N., Poluektov, O. G., Thurnauer, M. C., Schiffer, M., and Laible, P. D. (2003) Lysine substitutions near photoactive cofactors in the bacterial photosynthetic reaction center have opposite effects on the rate of triplet energy transfer. *Chem. Phys. 294*, 329–346.
32. McAuley-Hecht, K. E., Fyfe, P. K., Ridge, J. P., Prince, S. M., Hunter, C. N., Isaacs, N. W., Cogdell, R. J., and Jones, M. R. (1998) Structural studies of wild type and mutant reaction centres from an antenna-deficient strain of *Rhodobacter sphaeroides*: Monitoring the optical properties of the complex from cell to crystal. *Biochemistry 37*, 4740–4750.
33. Jones, M. R., Fowler, G. J. S., Gibson, L. C. D., Grief, G. G., Olsen, J. D., Crielaard, W., and Hunter, C. N. (1992) Construction of mutants of *Rhodobacter sphaeroides* lacking one or more pigment-protein complexes and complementation with reaction-centre, LH1, and LH2 genes. *Mol. Microbiol. 6*, 1173–1184.
34. Jones, M. R., Heer-Dawson, M., Mattioli, T. A., Hunter, C. N., and Robert, B. (1994) Site-specific mutagenesis of the reaction centre from *Rhodobacter sphaeroides* studied by Fourier transform Raman spectroscopy: Mutations at tyrosine M210 do not affect the electronic structure of the primary donor. *FEBS Lett. 339*, 18–24.
35. Frolov, D., Gall, A., Lutz, M., and Robert, B. (2002) Structural asymmetry of bacterial reaction centers: A Q_y resonant Raman study of the monomer bacteriochlorophylls. *J. Phys. Chem. A 106*, 3605–3613.
36. Gradinaru, C. C., van Stokkum, I. H. M., Pascal, A. A., van Grondelle, R., and van Amerongen, H. (2000) Identifying the pathways of energy transfer between carotenoids and chlorophylls in LHCII and CP29. A multicolor, femtosecond pump-probe study. *J. Phys. Chem. B 104*, 9330–9342.
37. Frolov, D., Wakeham, M. C., Andrizhiyevskaya, E. G., Jones, M. R., and van Grondelle, R. (2005) Investigation of B-branch electron transfer by femtosecond time resolved spectroscopy in a *Rhodobacter sphaeroides* reaction centre that lacks the Q_A ubiquinone. *Biochim. Biophys. Acta 1707*, 189–198.
38. van Stokkum, I. H. M., Scherer, T., Brouwer, A. M., and Verhoeven, J. W. (1994) Conformational dynamics of flexibly and semirigidly bridged electron donor-acceptor systems as revealed by spectrotemporal parametrization of fluorescence. *J. Phys. Chem. 98*, 852–866.
39. Kabsch, W. (1993) Automatic processing of rotation diffraction data from crystals of initially unknown symmetry and cell constants. *J. Appl. Crystallogr. 26*, 795–800.
40. Navaza, J. (1994) AMORE: An automated package for molecular replacement. *Acta Crystallogr. A50*, 157–163.
41. Murshudov, G. N., Vagin, A. A., and Dodson, E. J. (1997) Refinement of macromolecular structures by the maximum- likelihood method. *Acta Crystallogr. D53*, 240–255.
42. Evans, T. A., and Katz, J. J. (1975) Evidence for 5-coordinated and 6-coordinated magnesium in bacteriochlorophyll-a from visible absorption spectroscopy. *Biochim. Biophys. Acta 396*, 414–426.
43. Callahan, P. M., and Cotton, T. M. (1987) Assignment of bacteriochlorophyll *a* ligation state from absorption and resonance raman spectra. *J. Am. Chem. Soc. 109*, 7001–7007.
44. Hartwich, G., Fiedor, L., Simonin, I., Cmiel, E., Schäfer, W., Noy, D., Scherz, A., and Scheer, H. (1998) Metal-Substituted Bacteriochlorophylls. 1. Preparation and Influence of Metal and Coordination on Spectra. *J. Am. Chem. Soc. 120*, 3675–3683.
45. Van der rest, M., and Gringas, G. (1974) The pigment complement of the photosynthetic reaction centre isolated from *Rhodospirillum rubrum*. *J. Biol. Chem. 249*, 6446–6453
46. Näveke, A., Lapouge, K., Sturgis, J. N., Hartwich, G., Simonin, I., Scheer, H., and Robert, B. (1997) Resonance-Raman spectroscopy of metal-substituted bacteriochlorophylls: Characterisation of Raman bands sensitive to bacteriochlorin conformation. *J. Raman Spectrosc. 28*, 599–604.
47. Lapouge, K., Näveke, A., Sturgis, J. N., Hartwich, G., Renaud, D., Simonin, I., Lutz, M., Scheer, H., and Robert, B. (1998) Non-bonding molecular factors influencing the stretching wavenumbers of the conjugated carbonyl groups of bacteriochlorophyll *a*. *J. Raman Spectrosc. 29*, 977–981.
48. Beekman, L. M. P., Visschers, R. W., Monshouwer, R., Heer-Dawson, M., Mattioli, T. A., McGlynn, P., Hunter, C. N., Robert, B., Van Stokkum, I. H. M., Van Grondelle, R., and Jones, M. R. (1995) Time-resolved and steady-state spectroscopic analysis of membrane-bound reaction centers from *Rhodobacter sphaeroides*: Comparisons with detergent-solubilized complexes. *Biochemistry 34*, 14712–14721.
49. Beekman, L. M. P., van Stokkum, I. H. M., Monshouwer, R., Rijnders, A. J., McGlynn, P., Visschers, R. W., Jones, M. R., and van Grondelle, R. (1996) Primary electron transfer in membrane-bound reaction centers with mutations at the M210 position. *J. Phys. Chem. 100*, 7256–7268.
50. van Brederode, M. E., van Mourik, F., van Stokkum, I. H. M., Jones, M. R., and van Grondelle, R. (1999) Multiple pathways for ultrafast transduction of light energy in the photosynthetic reaction center of *Rhodobacter sphaeroides*. *Proc. Natl. Acad. Sci. U.S.A. 96*, 2054–2059.
51. Katilius, E., Katiliene, Z., Lin, S., Taguchi, A. K. W., and Woodbury, N. W. (2002) B side electron transfer in a *Rhodobacter sphaeroides* reaction center mutant in which the B side monomer bacteriochlorophyll is replaced with bacteriopheophytin: Low-temperature study and energetics of charge-separated states. *J. Phys. Chem. B 106*, 1471–1475.
52. Kirmaier, C., Gaul, D., Debey, R., Holten, D., and Schenck, C. C. (1991) Charge separation in a reaction center incorporating bacteriochlorophyll for photoactive bacteriopheophytin. *Science 251*, 922–927.
53. Wakeham, M. C., Goodwin, M. G., McKibbin, C., and Jones, M. R. (2003) Photo-accumulation of the $P^+Q_B^-$ radical pair state in purple bacterial reaction centres that lack the Q_A ubiquinone. *FEBS Lett. 540*, 234–240.
54. Ridge, J. P., van Brederode, M. E., Goodwin, M. G., van Grondelle, R., and Jones, M. R. (1999) Mutations that modify or exclude binding of the Q_A ubiquinone and carotenoid in the reaction center from *Rhodobacter sphaeroides*. *Photosynth. Res. 59*, 9–26.
55. Potter, J. A., Fyfe, P. K., Frolov, D., Wakeham, M. C., van Grondelle, R., Robert, B., and Jones, M. R. (2005) Strong effects of an individual water molecule on the rate of primary charge separation in the *Rhodobacter sphaeroides* reaction centre. *J. Biol. Chem. 280*, 27155–27164.
56. Mattioli, T. A., Lin, X., Allen, J. P., and Williams, J. C. (1995) Correlation between multiple hydrogen-bonding and alteration of the oxidation potential of the bacteriochlorophyll dimer of reaction centers from *Rhodobacter sphaeroides*. *Biochemistry 34*, 6142–6152.
57. Schenkl, S., Spörlein, S., Müh, F., Witt, H., Lubitz, W., Zinth, W., and Wachtveitl, J. (2002) Selective perturbation of the second electron transfer step in mutant bacterial reaction centers. *Biochim. Biophys. Acta 1554*, 36–47.
58. BenShem, A., Frolow, F., and Nelson, N. (2004) Evolution of photosystem I: From symmetry through pseudosymmetry to asymmetry. *FEBS Lett. 564*, 274–280.
59. Geskes, C., Hartwich, G., Scheer, H., Mäntele, W., and Heinze, J. (1995) An electrochemical and spectroelectrochemical investigation of metal-substituted bacteriochlorophyll a. *J. Am. Chem. Soc. 117*, 7776–7783.
60. Noy, D., Fiedor, L., Hartwich, G., Scheer, H., and Scherz, A. (1998) Metal-substituted bacteriochlorophylls. 2. Changes in redox potentials and electronic transition energies are dominated by intramolecular electrostatic interactions. *J. Am. Chem. Soc. 120*, 3684–3693.